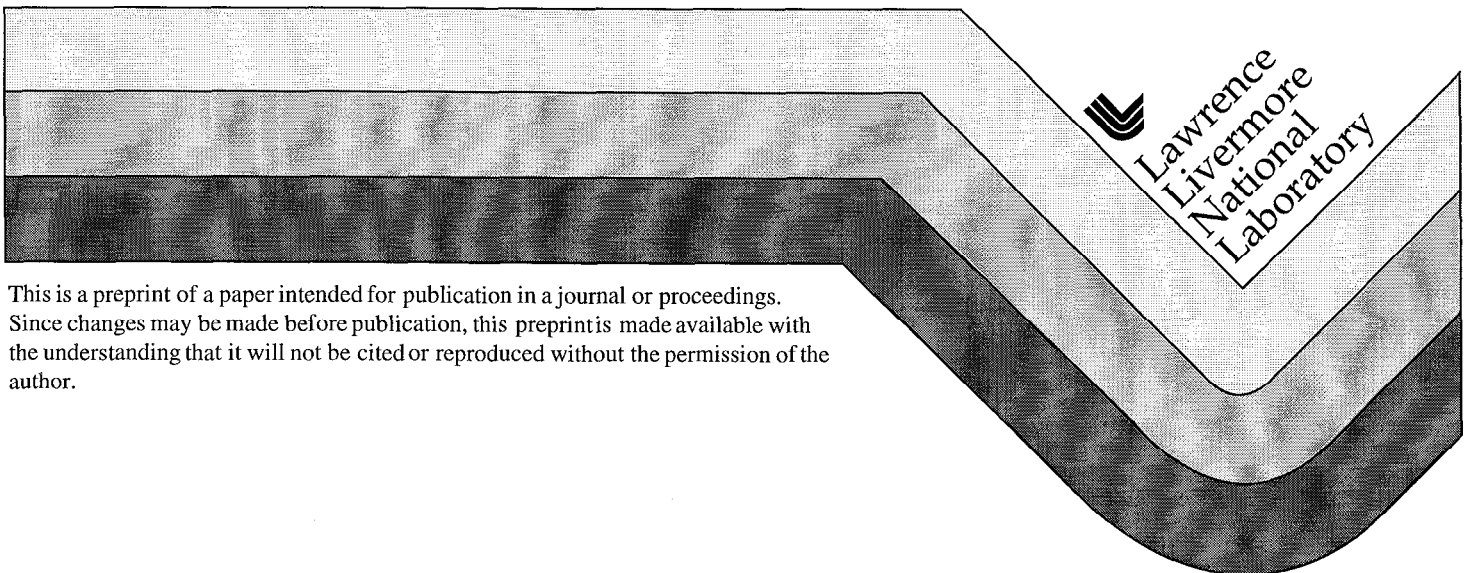# Simulation of an EBPVD Titanium Vapor Plume and Comparison to Experiment

D. G. Braun, T. M. Anklam,
L. V. Berzins, D. T. Blackfield,
M. A. McClelland, T. C. Meier,
K. W. Westerberg, I. Boyd,
J. Balakrishnan

DISCLAIMER

Simulation of an EBPVD Titanium Vapor Plume and Comparison to Experiment[*]

D. G. Braun[**]
T. M. Anklam
L. V. Berzins
D. T. Blackfield
M. A. McClelland
T. C. Meier
K. W. Westerberg

Lawrence Livermore National Laboratory
P.O. Box 808
Livermore, CA 94550 USA

I. Boyd
J. Balakrishnan

Sibley School of Mechanical and Aerospace Engineering
Cornell University
Ithaca, NY 14853 USA

Abstract

A 2 dimensional vapor code has been used to simulate the electron-beam vaporization of Titanium and its subsequent deposition on a horizontal substrate in experiments performed at Lawrence Livermore National Laboratory (LLNL). Previous work has modeled the Titanium melt. Using those results, the present work models the expansion of the atomic vapor from the melt surface to the substrate. The flow speed of the vapor expansion and its kinetic and internal temperatures were measured in the LLNL experiment as a function of the vaporization rate and the electron-beam footprint. The deposition profile on the substrate was also measured post-run. This work describes the experimental configuration and compares the measured quantities to those of the computer simulation.

1. Introduction

Electron Beam Physical Vapor Deposition (EBPVD) of materials has been used for a variety of industrial applications, including coating fibers with metal matrix composites [1] and producing thermal barrier coatings on turbine blades. In the EBPVD process, a high energy electron beam is used to heat a pool of liquid metal to the point of vaporization. The vaporized atoms undergo a hypersonic expansion from the surface of the pool to a (relatively) cold surface above where they are deposited, producing the desired coating. Key elements to making an EBPVD process economically viable are the amount of material vaporized per unit beam power (source efficiency) and the fraction of vapor that impinges on the deposition surface (vapor utilization).

To understand and then optimize the EBPVD process Lawrence Livermore National Laboratory (LLNL) has developed a model of the liquid pool and, in conjunction with Cornell University, a model of the expanding vapor plume. A primary objective of this research is the benchmarking of these models against Titanium vaporization experiments performed at LLNL. The pool model and its results have been presented elsewhere [2]. This work will describe the vapor model and the comparison of its results to the measured values.

2. Experimental Geometry and Vapor Properties Measurement

The Titanium vaporization experiments were performed in the Evaporation Test Facility (ETF) at LLNL. A schematic of ETF is shown in Fig. 1. A 3" diameter bar of Titanium was bottom fed into a water cooled copper crucible. A 33 keV electron beam was bent 90° on to the surface of the bar by a localized magnetic field produced using a solenoid coil with end plates. Melt view cameras inside the vessel provided images of the Titanium pool and the beam footprint. The electron beam spot size was approximately 0.5" in diameter. Using a pair of deflection coils, the spot was swept across the melt surface in a circular pattern. Two ring diameters were typically used for the vaporization experiments; 1.85" and 0.95". The beam was swept at a frequency of 3-4 kHz, sufficiently fast so that there were no time dependent vapor fluctuations associated with the liquid cooling between passes of the electron beam.

As shown in Fig. 1, a deposition substrate was placed 18" above the Titanium source. Light from diagnostic lasers propagated through the vapor above and below the substrate, on the centerline of the system, at standoffs of 15" and 19" above the melt surface. The vapor density in the laser paths was determined from the absorption profile produced when the frequency of the diagnostic lasers was swept through a known atomic transition (see [3] for a discussion of the technique). Two symmetric slots were cut in the substrate extending from 5.5" to 7.5" from the centerline. Assuming radial flow from the center of the liquid pool, the vapor passes through the slots at angles of ±20° from vertical. As a result the 2 absorption peaks measured at the upper laser shot are Doppler shifted to frequencies above and below the transition center. The flow speed of the vapor is then determined from

$$\Delta f * \lambda = u * \sin\left(20°\right) ,$$

where Δf is the frequency shift and λ is the wavelength of the laser light.

Upper Laser Shot   - y = 19"

Substrate   y = 18"

Lower Laser Shot   - y = 15"

Deflection
Coils

Electron
Beam

3" Titanium Rod
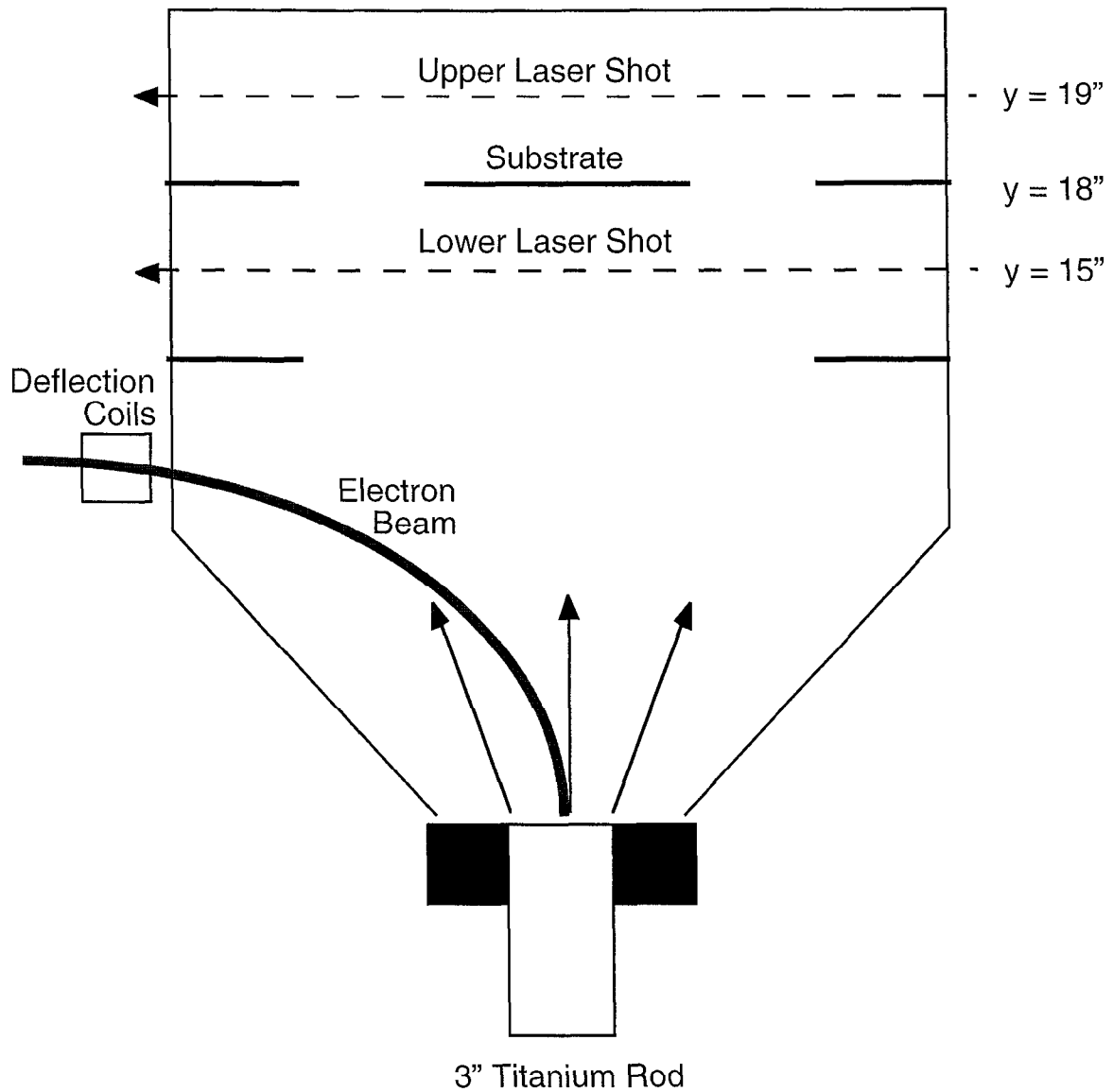
Figure 1. A schematic view of the ETF vaporizer showing the locations of the diagnostic lasers, the deposition substrate, the electron gun and the bottom feed source.

The width of the 2 absorption peaks measured at the upper location is also Doppler broadened by the spread of velocities within the vapor. Assuming a Maxwellian distribution, the kinetic or translational temperature of the vapor, T_{tr}, is obtained from the measured full-width-half-max of the absorption peak according to

$$\text{FWHM} = \frac{2}{\lambda}\left(\frac{2kT_{tr}}{m}\ln 2\right)^{1/2},$$

where m is the atomic mass of Titanium and k is Boltzmann's constant.

At the location below the substrate light was propagated from two diagnostic lasers tuned to atomic transitions out of the ground state of Titanium and out of its first excited state (170 cm^{-1}). From the measured densities of the two states, the internal or electronic temperature of the vapor, T_e, can be evaluated from Boltzmann's relation

$$\frac{n_1}{n_o} = \frac{g_1}{g_0} \exp\left(-\frac{E_1}{kT_e}\right) ,$$

where E_1 is the excitation energy of the first excited state and g_o and g_1 are the atomic degeneracies of the ground and first states.

The characterization of the vapor plume was completed with the evaluation of its spatial profile, as determined from post-run thickness measurements of the substrate deposit. Whereas the vapor flow speed, the translational temperature and the internal temperature were measured with the diagnostic lasers every 10 s during the experiments (and thus record the changing conditions of the vapor plume), the deposition profile reflects the run integrated vapor profile. An alternate method for measuring the vapor profile in real time would be to look at the ratio of the density measured above the slot to the line integrated density measured below. A smaller ratio indicates a narrower profile, while a larger ratio represents a broader vapor distribution. Unfortunately, although the upper shot's absorption traces were adequate for determining the flow speed and translational temperature, the integrated signal used to determine the density contained significant noise. As a result, the spatial profile could accurately be determined only from the more restrictive post-run measurement.

The vapor characterization experimemts consisted of 2 ETF runs, 9703 and 9704, whose run conditions are summarized in Table 1. In the first, the electron beam operation was unchanged so that the vapor profile corresponding to those conditions could be determined. The second run contained three different vaporization periods in which the beam power and footprint were varied. The goal of that run was to measure the changes in vapor velocity and temperatures that were produced by the different source conditions. Note that although the steady state conditions of Run 9703 were identical to those used in the first period of Run 9704, the vaporization rates produced differed by 7%. This is typical of the run-to-run variation observed in the ETF source efficiency.

Run	Beam Current (A)	Beam Power (W)	Beam Footprint Diameter (in)	Measured Vapor Rate (kg Ti/h)
9703	1.18	38.2	1.85	1.05
9704 - A	1.18	38.6	1.85	1.12
9704 - B	1.29	42.6	1.85	1.48
9704 - C	1.18	38.8	0.95	1.29

Table 1. The beam operating conditions used in ETF Runs 9703 and 9704, and the resulting vaporization rates.

The measured ground state density in Run 9704 is shown in Fig. 2. The density and vapor rate increased between run periods A and B as the beam current was raised from 1.18 to 1.29 A. In both these first run periods a 1.85" diameter beam footprint was used. In run period C the beam current was returned to 1.18 A, but the source diameter was reduced to 0.95". This concentration of power produced higher source temperatures and increased local vaporization rates, which more than offset the reduced area of the footprint. As a result, this geometry produced vapor densities comparable to those measured in run period B even at the lower beam power.

The measured translational and internal temperatures for run 9704 are shown in Fig. 3 and 4. Neither temperature changes significantly between run periods A and B as the beam current was increased. The apparent explanation is that the additional beam power produced a small relative increase in the source temperature, so that the far-field temperatures in the vapor were unchanged. However, since the evaporation rate is exponential in temperature, this small relative increase in the source temperature was still sufficient to produce a ~30% increase in the vaporization rate.

Both the translation and internal temperatures decreased when the beam footprint diameter is reduced to 0.95" in run period C. This is consistent with the theory of isentropic expansions, which states that the amount of vapor cooling increases with the ratio of
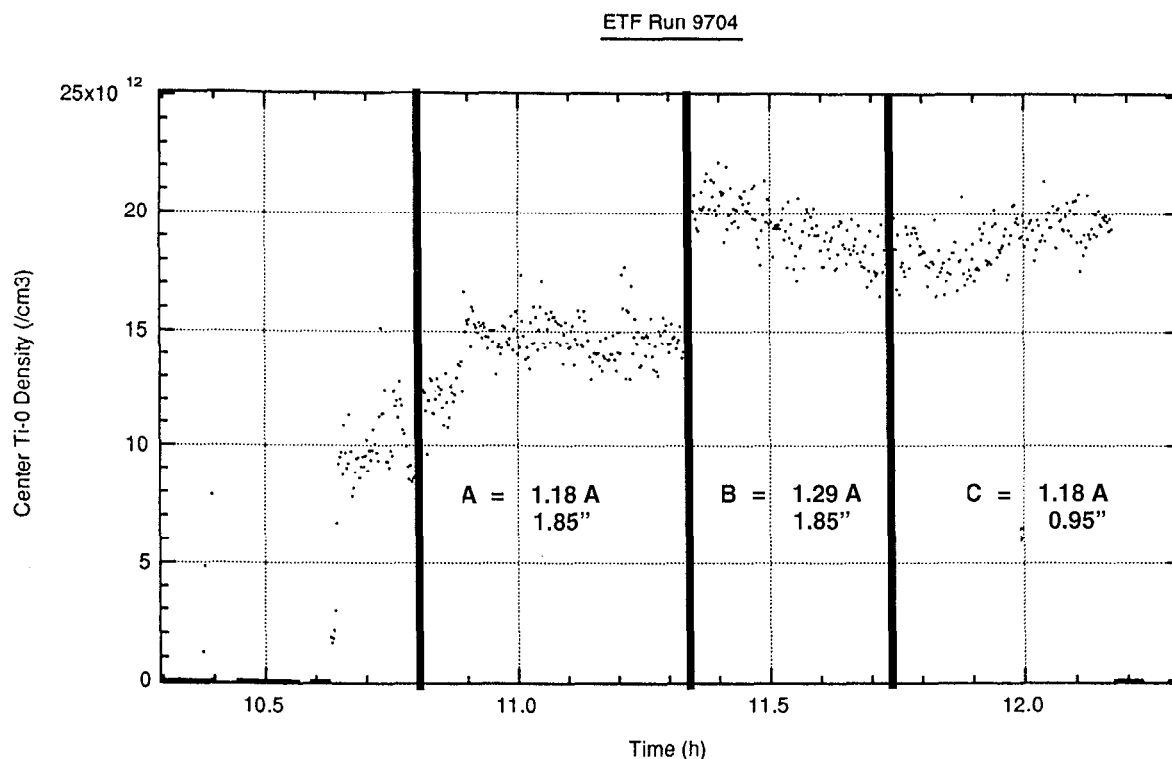

Figure 2. The measured ground state density at the lower laser shot versus time in ETF Run 9704.
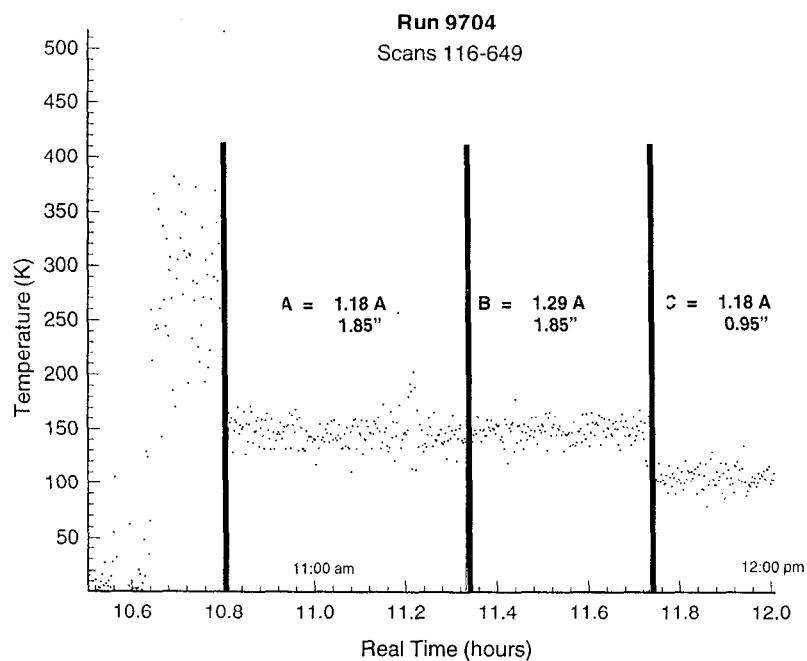
Figure 3. The vapor translational temperature measured at the upper laser shot versus time in ETR Run 9704.
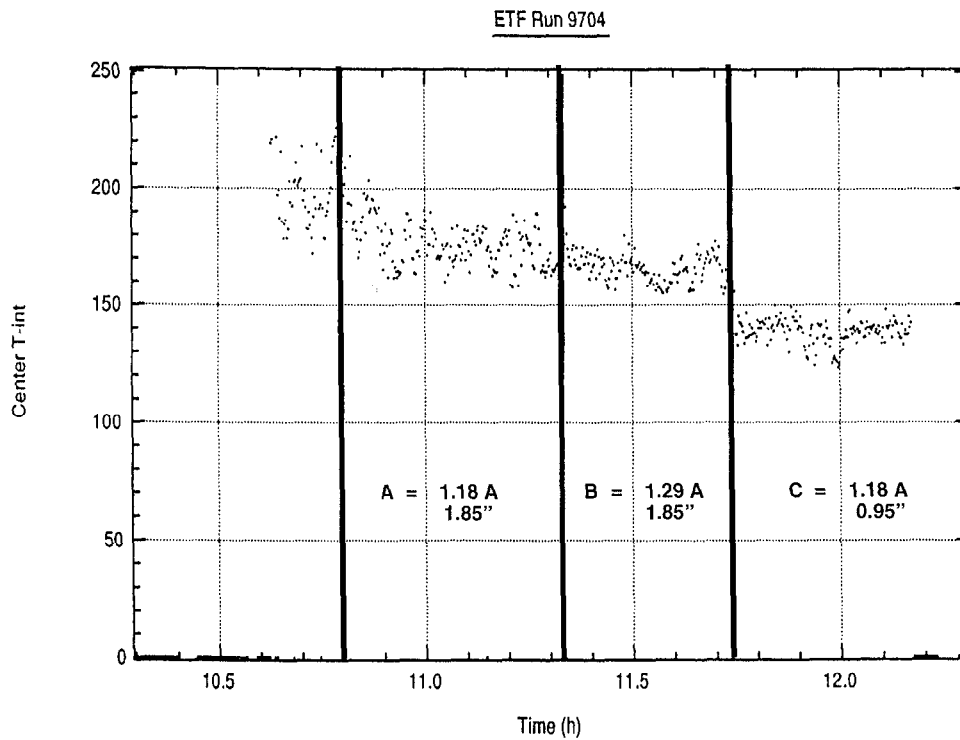

Figure 4. The vapor electronic temperature (K) measured at the lower laser shot versus time in ETF Run 9704.
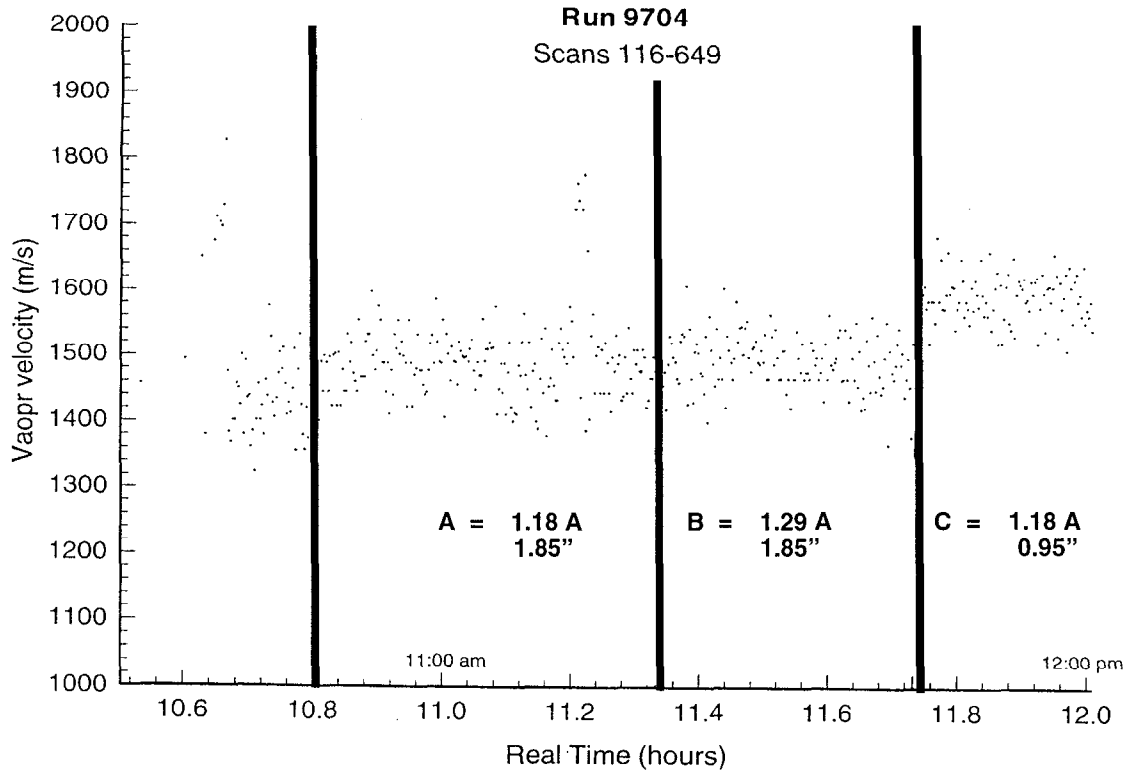
Figure 5. The vapor flow speed measured at the upper laser shot versus time in ETF Run 9704.

initial to final flow stream area (e.g. see [4]). With the smaller source diameter, this expansion ratio is greater in run period C than it was in periods A and B. The observed temperature decrease is especially noteworthy in that the initial vapor temperature (i.e. the source temperature) was greater in run period C with the reduced footprint diameter.

The measured vapor flow speed for Run 9704 is shown in Fig. 5. Again, no significant change is observed between run periods A and B. This reflects the above mentioned fact that the relative change in the source temperature is small. There is a noticeable change in the flow speed during run period C. This reflects the greater source temperatures and input energy that were produced when the ring diameter was decreased.

3. Vapor Model Description

The vapor plume was modeled with the Monaco code developed at Cornell University, which uses the Direct Simulation Monte Carlo technique [5]. A 2 dimensional code capable of modeling axisymmetric flows, Monaco partitions the flow field into cells that are typically

1 mean free path in size. (Note; this requires an iteration of the grid since the mean free paths are not known a priori.) The code simulates vaporization by launching particles from the melt surface by random sampling from a half-Maxwellian distribution of initial velocities. The radial profile of the liquid surface, the local surface temperature and the magnitude of the local evaporation flux are taken from the results of the melt modeling. Monaco then follows the particles recalculating their positions over a number of short time steps until they are collected on an absorbing surface. In the ETF simulations, all of the surfaces are assumed to be perfectly absorbing, including the liquid source.

At each time step Monaco tallies the particles in the simulation cells and evaluates the local vapor properties. From the collision cross-section (which is the one free parameter in the simulation) and the local vapor density the number of collisions in each cell over the time step is evaluated. Collision pairs are chosen at random and the particle pair is elasticly scattered. The process of moving particles and performing scattering collisions is iterated over many time steps. After equilibrium flow is established, Monaco accumulates the cell data over subsequent time steps, averaging the data to produce the desired vapor properties in the cell. This average is taken over many samples to reduce the statistical scatter in the results and converge to the final flow properties.

A key addition to the Monaco simulations is the inclusion of the electronic energy of the atoms. In equilibrium, the density of atoms in each electronic state is described by Boltzmann's distribution

$$\frac{n_i}{n_{total}} = \frac{g_i \exp\left(-\dfrac{E_i}{kT_e}\right)}{\sum_j g_j \exp\left(-\dfrac{E_j}{kT_e}\right)} \ ,$$

where the sum is performed over all the states and g_i is again the degeneracy of the ith state. Previous measurements on various elements have demonstrated that due to the high source temperatures characteristic of EBPVD, a significant portion of the flow energy can be contained in the electronic states of the atoms [6]. For Titanium, it is estimated that electronic energy adds approximately 6-8% to the flow energy. It is therefore an important effect to include.

An important simplification used in the Monaco simulations is the merging of the electronic states that have approximately the same energy. Typically the states that are merged have an energy difference of less than 5%. The degeneracies of the merged states are added together so that the correct number of excited particles is obtained with only a very slight error in the total energy. The merged electronic states used in the Titanium simulations are given in Table 2. In this case, the number of excited states has been reduced from 27 (the actual number below 17300 cm^{-1}) to 11. Typically all 11 states are allowed in the simulation to permit the rare high energy atom in the tail of the Boltzmann distribution.

When the simulation particles are launched they are assigned an electronic energy based on the above distribution and the local surface temperature of the melt. In the particle collisions, the Borgnakke-Larsen scheme [7,8] is applied to determine the post-collision electronic energy levels of the particles. In this scheme the final states are chosen at random from the Maxwell-Boltzmann distribution of levels evaluated at the total energy of the colliding

Level	Energy (K)	Degeneracy
1	0.00	5
2	244.79	7
3	556.65	9
4	9612.17	35
5	10439.89	5
6	12245.26	9
7	16761.80	21
8	17436.53	9
9	20264.21	15
10	21815.48	27
11	23218.71	45

Table 2. The electronic energy states for Titanium used in the Monaco simulations of the ETF vaporization experiments.

---

particles. This technique replaces a detailed quantum mechanical calculation of the various inelastic collision cross-sections, which besides being a formidable task would still contain considerable uncertainty. The benefit of such a model is that it accounts for the electronic energy of the particles and assures that they relax to the correct equilibrium distribution. It should be noted that similar schemes have been previously used to model electronic energy transfer [9,10,11] .

Simulation results for the case of the 1.85" diameter ring and the 1.18 A beam current are shown in Fig. 6. It can be seen that the vapor expansion occurs very quickly, as by 10 cm above the melt the vapor temperatures have fallen to less than 500 K and the flow speed is over 1200 m/s. Both values are near their far field values. It is interesting to note that the flow speed peaks off-axis. The reason for this is shown in Fig. 7, which shows the density and flow speed contours near the source. Inside the ring source there is initially no expansion as the vapor flow is essentially planar. Expansion (and its accompanied vapor cooling) occurs only along the stream lines at the outside edge of the ring source. It is this effect that produces the off-axis velocity peak.

4. Comparison of Simulation Results to the Experimental Data

Vapor simulations were performed for ETF Run 9703 and each of the 3 source configurations used in Run 9704. Each simulation used the surface profile and the local source temperature and vaporization rates calculated by the melt model. The value of the collision cross-section (hard sphere collisions, no energy dependence) was varied to provide the best agreement with the measured data. For the simulations shown here, a relatively large cross-section of $314 * 10^{-20}$ m^2 was used.

DENSITY (m^{-3})

Legend:
- 2.5E+21
- 1E+21
- 5E+20
- 2.5E+20
- 1E+20
- 5E+19
- 1E+19
- 5E+18
- 2.5E+18
- 1E+18

VELOCITY (m/s)

Legend:
- 1425
- 1400
- 1350
- 1300
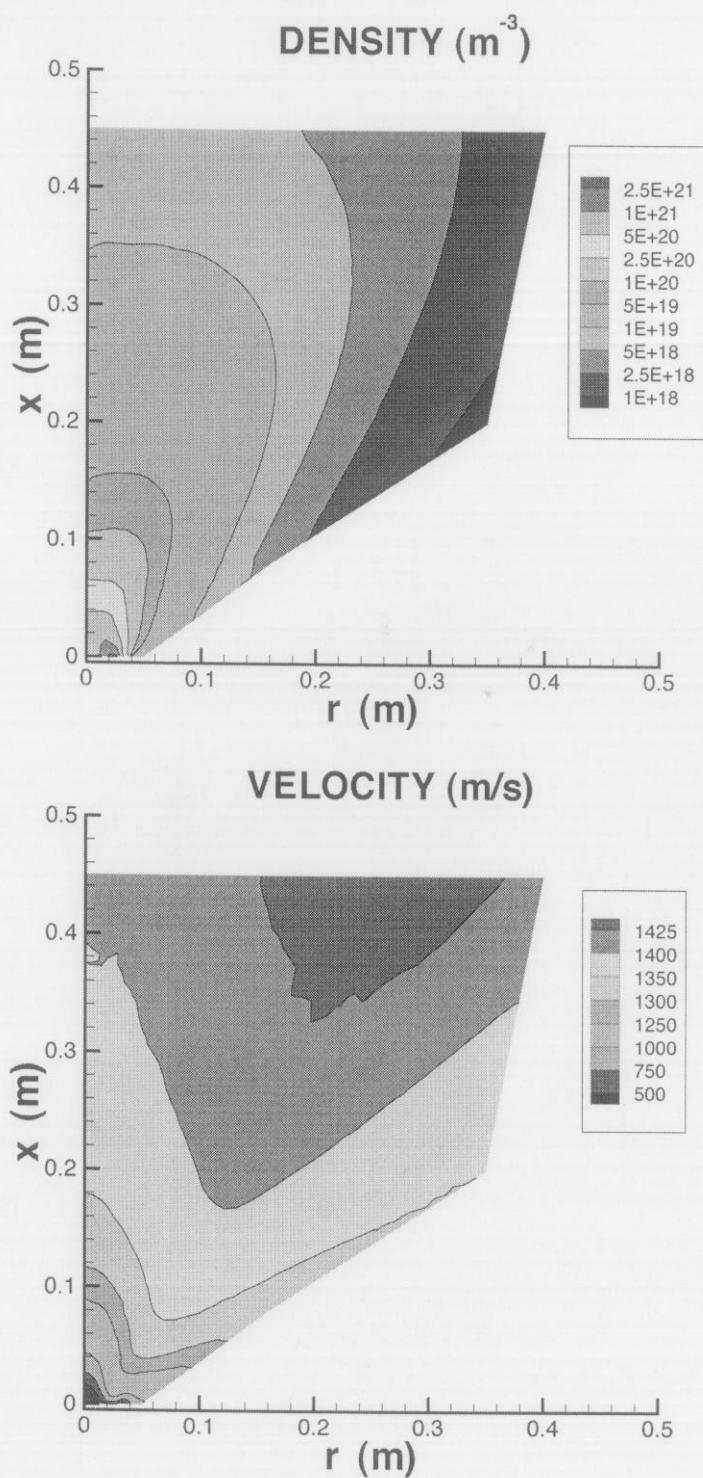- 1250
- 1000
- 750
- 500

Figure 6a. The density and flow speed of Titanium calculated by Monaco for the simulation with a 1.85" ring source and 1.18 A beam current.
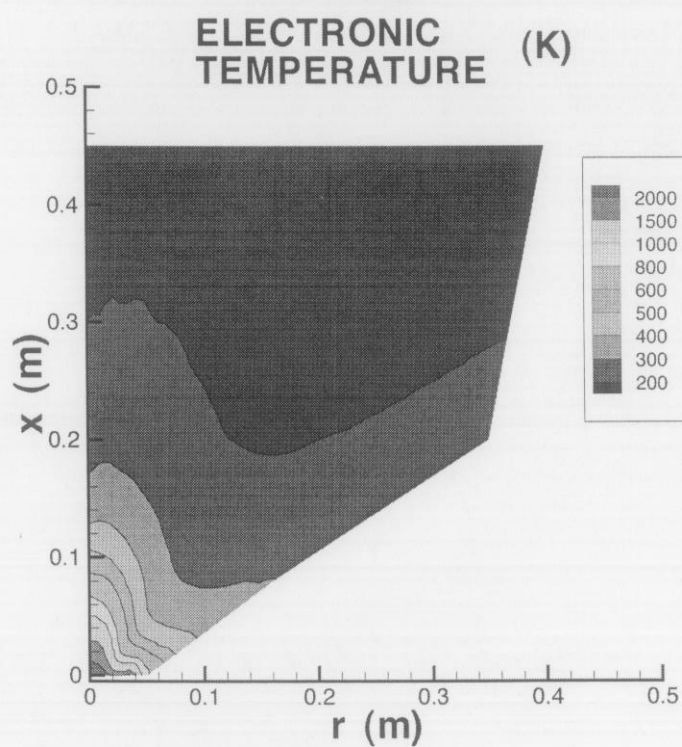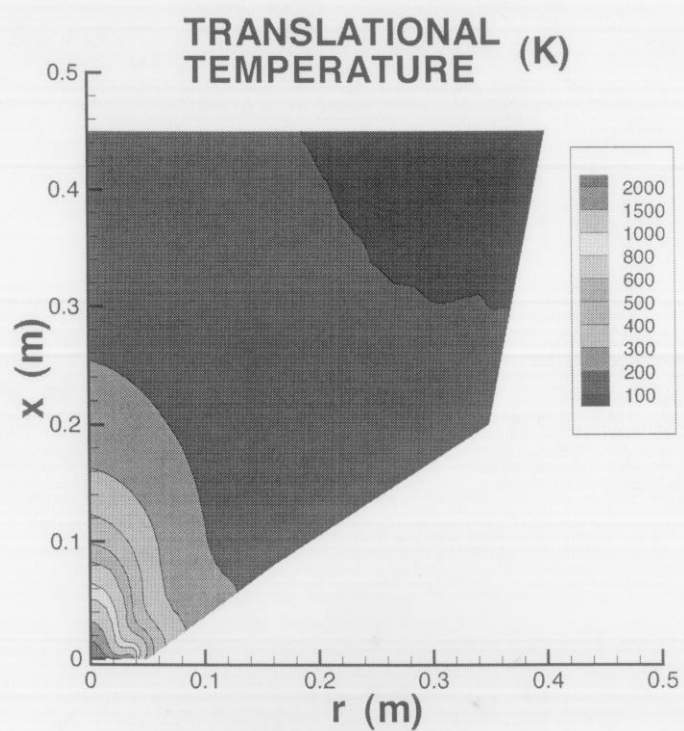
Figure 6b. The translation and electronic temperatures of Titanium calculated by Monaco for the simulation with a 1.85" ring source and 1.18 A beam current.
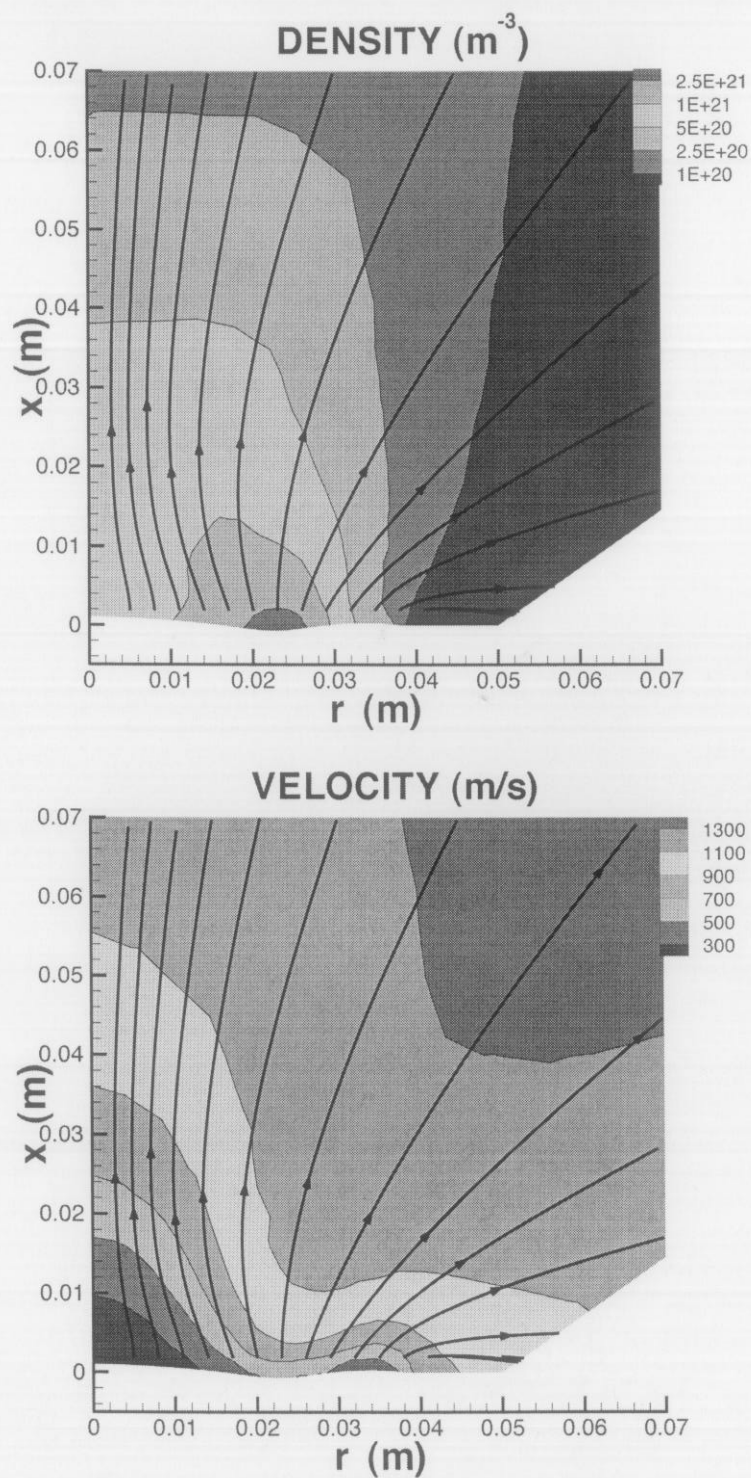
Figure 7. The density and flow speed of Titanium near the vapor source calculated by Monaco for the simulation with a 1.85" ring source and 1.18 A beam current. Also shown are the flow streamlines.

ETF 9703
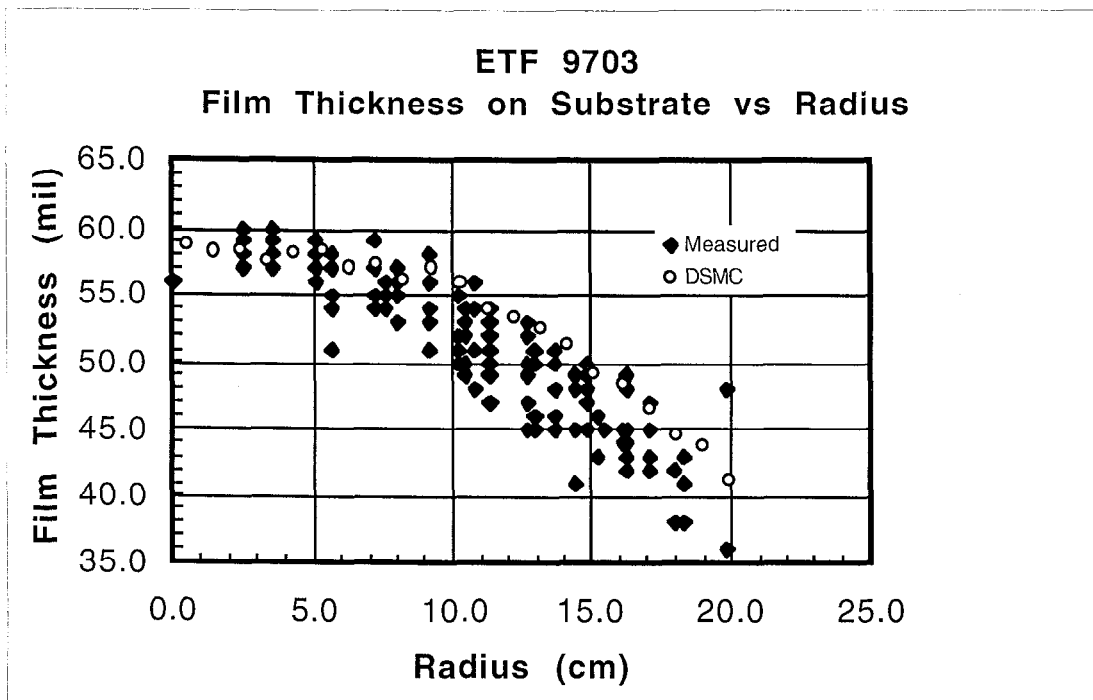## Film Thickness on Substrate vs Radius

Figure 8 The measured film thickness on the substrate in ETF Run 9703 versus radius from the centerline, compared to the normalized calculated profile from Monaco.

In Fig. 8 the calculated deposition profile on the substrate is compared to the film thickness measured after ETF Run 9703. Because of the axisymmetric geometry of the vapor plume, numerous thickness measurements were available at a given radius. The source of the relatively large scatter in the data points is not known. It is seen that the simulation results lie at the top edge of the run data. In the course of performing the simulations it was noted that adjusting the collision cross-section had an impact on the shape of the calculated profile. For example, using a perhaps more realistic cross-section of ~100 * 10^{-20} m^2, the calculated deposition profile went through the center of the measured data. That is, the simulation's vapor plume became broader as the number of collisions were increased.

The comparison of the measured and calculated vapor properties is shown in Table 3. It is seen that the qualitative dependence of the flow speed, translational and electronic temperatures on the source conditions is reproduced by the simulations. The reason for the use of 314 * 10^{-20} m^2 for the collision cross-section can also be seen, as it provides very good quantitative agreement between the measured and calculated electronic temperatures. Although they agree to within 10%, the calculated flow speeds are consistently less than the measured values. This indicates that the total energy of the simulation's particles is still low. Some of this energy will be provided when the source temperatures are increased to account for backscattered particles, as will be discussed in the following section. Another energy source is the collisional excitation of the vapor atoms by the energetic beam electrons enroute to the melt surface. This effect has previously been reported in Gadolinium flow speed measurements [12]. Since an electronic energy model is in the simulations, including this effect will be a relatively straight forward addition.

Beam Current (A)	Vapor Rate (kg/h)	Source Diameter (in)	Vapor Velocity (m/s)		Kinetic Temperature (K)		Electronic Temperature (K)	
			Measured	Calculated	Measured	Calculated	Measured	Calculated
1.18	1.12	1.85	1490	1421	145	94	175	181
1.29	1.48	1.85	1510	1437	150	97	165	176
1.18	1.29	0.95	1600	1500	105	62	140	125

Table 3. Comparison of the measured and calculated vapor properties for the 3 source operating conditions used in ETF Run 9704.

5. Corrections to the Melt Model

The results of the melt model are reproduced from [2] in Fig. 9, where the calculated vaporization rate versus beam power is compared to the rate measured in a number of ETF runs that used the 1.85" diameter source. As an ab initio calculation of the vapor rate versus electron beam power, the agreement between the calculation and experiment is good. The calculated rate is approximately 80% greater than the measured rates, but the difference in the pool temperatures is much less (due to the exponential dependence of the vapor rate). As a possible source of the remaining discrepancy, uncertainty in the skip electron fraction was initially cited [2]. Although this is still true, the vapor simulations now provide additional corrections to the melt model through the evaluation of backscattered particles.
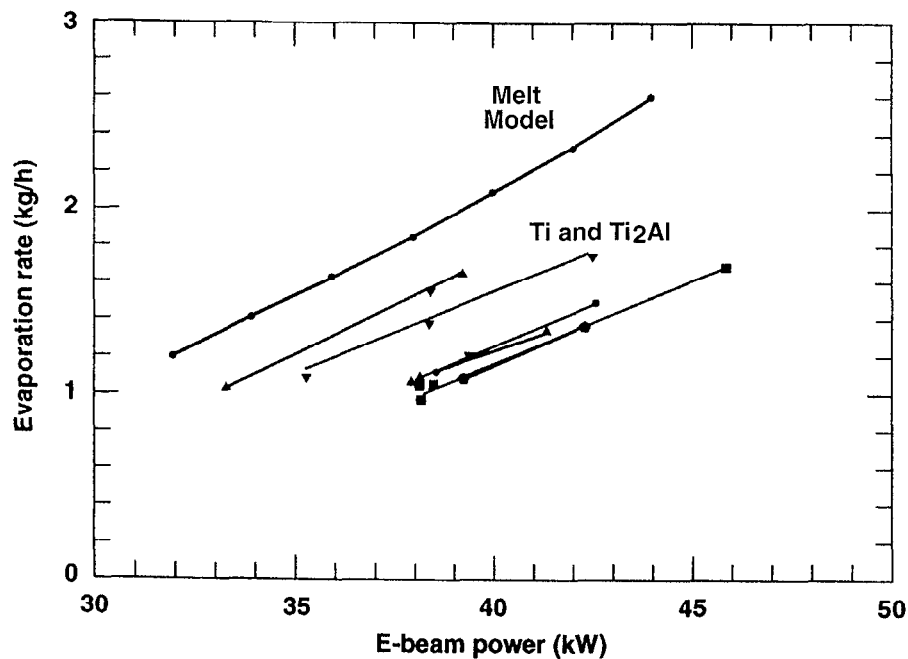

Figure 9. Comparison of measured Titanium vaporization rates versus beam power to those calculated by the Melt model, for a 1.85" diameter source.

The radial surface profile and the calculated vaporization flux density are shown in Fig. 10 for the case with the 1.85" ring source and the 1.18 A beam current. The hot zone under the beam footprint corresponds to the vaporization peak. It is primarily the thrust produced by particles leaving the liquid pool that produces the surface depression. Also shown is the flux density of particles that return to the liquid surface as a result of backscattering collisions in the vapor. The pool surface is assumed to be a perfect absorber of these particles. The backscatter peak coincides with the vaporization flux since backscattering can occur only in the first few collisions. As a result, the backscattered particles strike the melt very close to where they originated. In the simulations performed to date, the total backscatter fraction has been 16-22% of the net vaporization rate. This is a direct reduction to the calculated vaporization rate shown in Fig. 7, which did not include the backscatter correction.
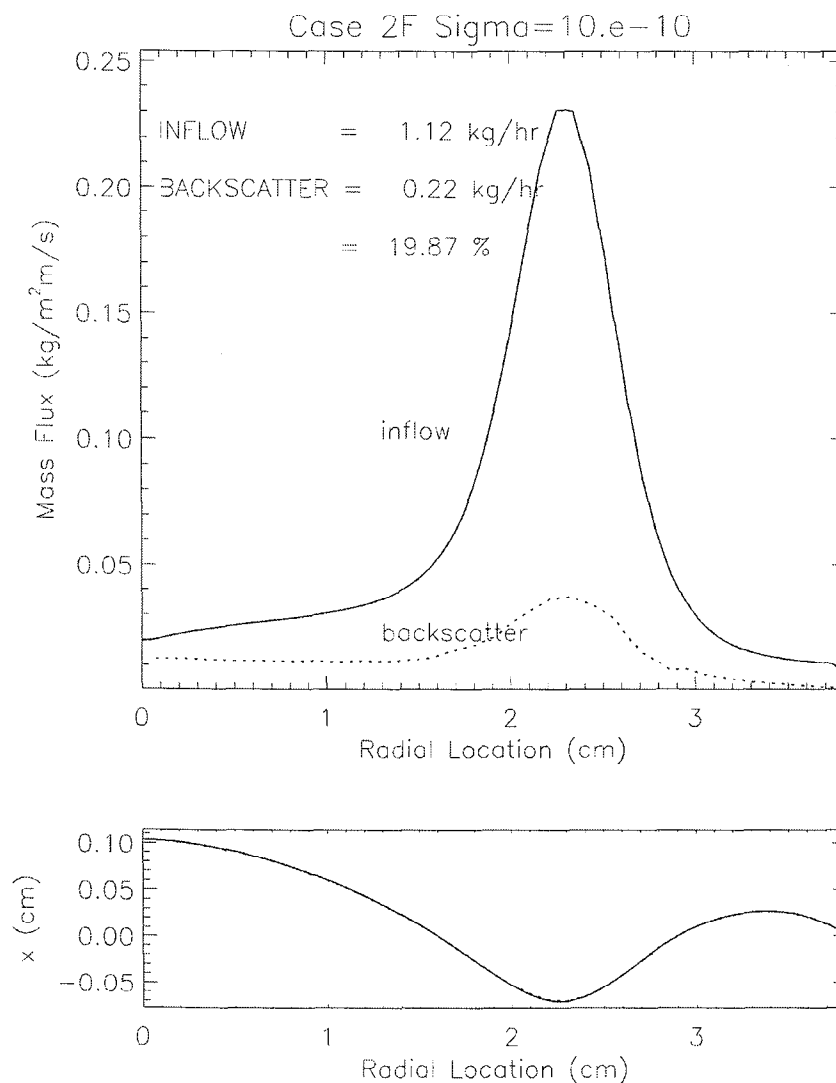

Figure 10. The calculated vaporization and backscatter flux of Titanium on the pool surface for the case with a 1.85" diameter footprint and a beam current of 1.18 A. The bottom plot shows the calculated surface profile of the melt.

When the backscattered particles strike the melt surface they impart their momentum to the liquid. The calculated normal (pressure) and tangential (shear) forces produced by the backscattered particles are shown in Fig. 11. The pressure force will tend to increase the depth of the liquid depression at the beam footprint. Its effect on the calculated vaporization rate is not known. The shear force acts to reinforce the natural circulation currents present in the liquid pool. These result from the temperature dependence of the liquid density (buoyancy) and surface tension (Marangoni effect). To the extent that the shear force increases the liquid's circulation, it will produce increased heat transfer to the cold crucible and lower vaporization rates for the same beam power. As such, including the shear force produced by the backscattered particles will also tend to bring the calculated and measured vapor rates into better agreement.
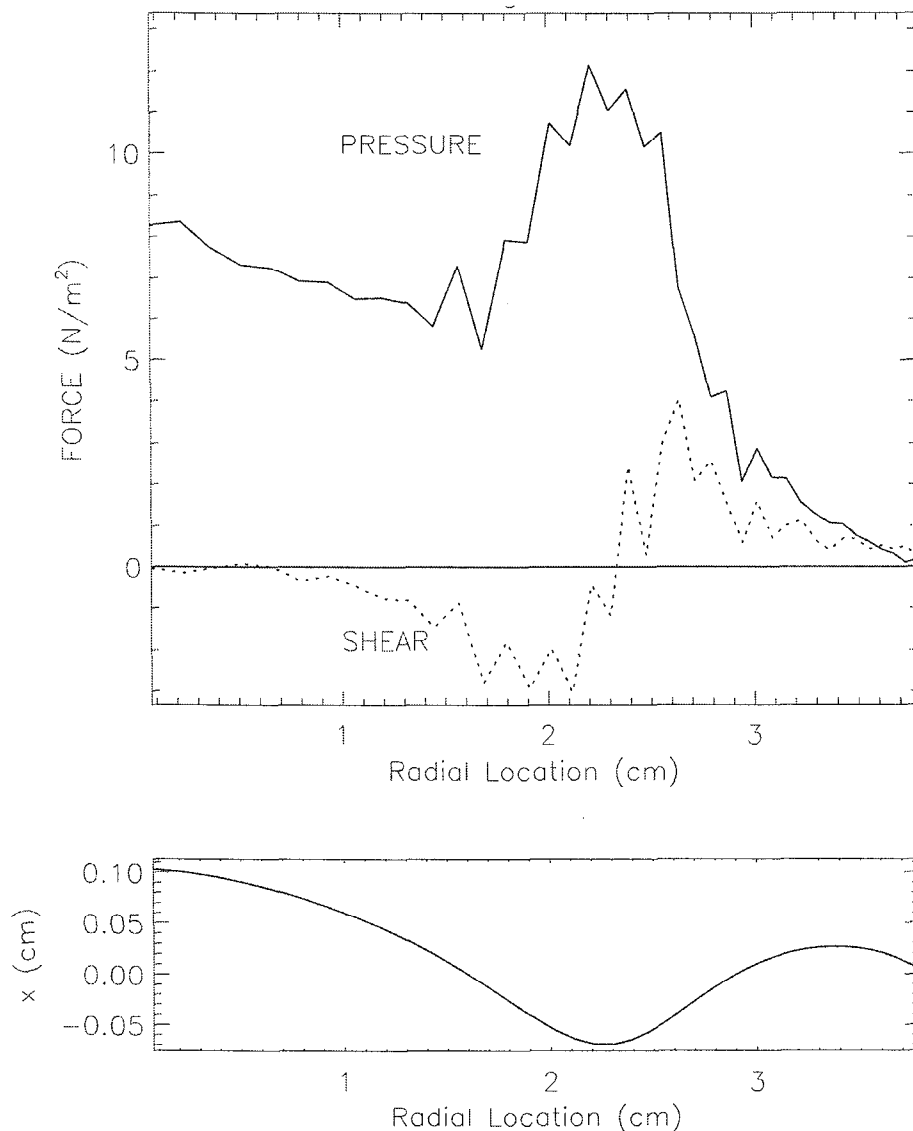

Figure 11. The calculated normal and tangential force (pressure and shear) imparted by the backscattered Titanium to the liquid pool for the case with a 1.85" diameter footprint and a beam current of 1.18 A. Bottom plot shows the calculated surface profile of the melt.

6. Summary and Future Work

A 2 dimensional vapor code has successfully been coupled to the LLNL melt model to perform simulations of Titanium vapor experiments. The agreement between the code results and the experimental data is good, although a number of things could be done to make the agreement even better. Future work will investigate the effect of collisional heating of the vapor by the electron beam. Iterations will also be performed between the melt and vapor codes to include the effects of backscattered particles and produce self-consistent models of the Titanium vaporization.

7. Acknowledgments

ST 98-208/DGB:dlb
L-24919-01

References

[1] J. Storer, "Electron Beam Deposition for the Fabrication of Titanium MMCs", in *Electron Beam Melting and Refining State of the Art 1993*, R. Bakish, editor, pages 235-245. Bakish Materials Corp., Englewood, NJ, 1993.

[2] K. Westerberg et al, "Analysis of the E-Beam Evaporation of Titanium and Ti-6Al-4V", in *Electron Beam Melting and Refining State of the Art 1997*, R. Bakish, editor, pages 208-221. Bakish Materials Corp., Englewood, NJ, 1997.

[3] L. Berzins, *Using Laser Absorption Spectroscopy to Monitor Composition and Physical Properties of Metal Vapors*, LLNL publication UCRL-JC-112979, and in the SPIE Proceedings of *Chemical, Biochemical, and Environmental Fiber Sensors V*, September, 1993.

[4] H.W. Liepmann and A. Roshko, *Elements of Gasdynamics*, Chapter 2, John Wiley and Sons, New York, 1957.

[5] G.A. Bird, *Molecular Gas Dynamics*, Clarendon Press, Oxford, 1994.

[6] J.L. Fleche et al, "Measurement and Interpretation of the Atomic Velocities Produced by Electron Bombardment", in *Rarefied Gas Dynamics; Experimental Techniques and Physical Systems*, B.D. Shizgal and D.P. Weaver editors, pages 66-67, Progress in Astronautics and Aeronautics Vol. 158, AIAA, Washington DC, 1994.

[7] C. Borgnakke and P.S. Larsen, "Statistical Collision Model for Monte Carlo Simulation of Polyatomic Gas Mixtures", *Journal of Computational Physics* 18, page 405, 1975.

[8] F. Bergemann and I.D. Boyd, "DSMC Simulation of Inelastic Collisions Using the Borgnakke-Larsen Method Extended to Discrete Distributions of Vibrational Energy",

in *Rarefied Gas Dynamics; Experimental Techniques and Physical Systems*, B.D. Shizgal and D.P. Weaver editors, pages 66-67, Progress in Astronautics and Aeronautics Vol. 158, AIAA, Washington DC, 1994.

[9] J. Anderson et al, "Statistical Theory of Electronic Energy Relaxation", in *Rarified Gas Dynamics*, V. Boffi and C. Cercignani editors, Vol. 1, pages 413-421, B.G. Teubner, Stuttgart, 1986.

[10] J.L. Fleche and C. Gonella, "DSMC Simulation of Overheating Through Atomic Inelastic Collisions in a Metal Vapour Jet Expansion", in *19ʰ International Symposium on Rarefied Gas Dynamics*, J. Harvey and G. Lord editors, Vol. 1, pages 542-548, Oxford, 1994.

[11] S. Chatain et al, J. Phys. D: Appl. Phys. **30**, page 360, 1997.

[12] A. Nishimura et al, J. Nuc. Sci. Tech., **29**, page 1054, 1992.